

Edge properties and Majorana fermions in the proposed chiral d -wave superconducting state of doped graphene

Annica M. Black-Schaffer

Department of Physics and Astronomy, Uppsala University, Box 516, S-751 20 Uppsala, Sweden

(Dated: September 18, 2018)

We investigate the effect of edges on the intrinsic d -wave superconducting state in graphene doped close to the van Hove singularity. While the bulk is in a chiral $d_{x^2-y^2} + id_{xy}$ state, the order parameter at any edge is enhanced and has $d_{x^2-y^2}$ -symmetry, with a decay length strongly increasing with weakening superconductivity. No graphene edge is pair breaking for the $d_{x^2-y^2}$ state and there are no localized zero-energy edge states. We find two chiral edge modes which carry a spontaneous, but not quantized, quasiparticle current related to the zero-energy momentum. Moreover, for realistic values of the Rashba spin-orbit coupling, a Majorana fermion appears at the edge when tuning a Zeeman field.

PACS numbers: 74.20.Rp, 74.70.Wz, 74.20.Mn, 73.20.At, 71.10.Pm

Graphene, a single layer of carbon, has generated immense interest ever since its experimental discovery [1]. Lately, experimental advances in doping methods [2, 3] have allowed the electron density to approach the van Hove singularities (VHSs) at 25% hole or electron doping. The logarithmically diverging density of states (DOS) at the VHS can allow non-trivial ordered ground-states to emerge due to strongly enhanced effects of interactions. Very recently, both perturbative renormalization group (RG) [4] and functional RG calculations [2, 6] have shown that a chiral spin-singlet $d_{x^2-y^2} + id_{xy}$ ($d_1 + id_2$) superconducting state likely emerges from electron-electron interactions in graphene doped to the vicinity of the VHS. This is in agreement with earlier studies of strong interactions on the honeycomb lattice near half-filling [1, 8–10].

Rather unique to the honeycomb lattice is the degeneracy of the two d -wave pairing channels [1, 11]. Below the superconducting transition temperature (T_c), this degeneracy results in the time-reversal symmetry breaking $d_1 + id_2$ state [1, 4]. However, any imperfections, and most notably edges, might destroy this degeneracy and generate a local superconducting state different from that in the bulk. At the same time, many of the exotic features proposed for a $d_1 + id_2$ superconductor, such as spontaneous [12, 13], or even quantized [14], edge currents and quantized spin- and thermal Hall effects [15, 16], are intimately linked to its edge states. In order to determine the properties of $d_1 + id_2$ superconducting graphene, it is therefore imperative to understand the effect of edges on the superconducting state.

In this Letter we establish the edge properties of $d_1 + id_2$ superconducting graphene doped to the vicinity of the VHS. We show that, while the bulk is in a $d_1 + id_2$ state, any edge will be in a pure, and enhanced, d_1 -wave state. Due to a very long decay length of the edge d_1 state, the edges influence even the properties of macroscopic graphene samples. We find two well-localized chiral edge modes which carry a spontaneous, but not quantized, edge current. Furthermore, we show that by including a realistic Rashba spin-orbit coupling, graphene can be tuned, using a Zeeman field, to host a Majorana fermion at the edge. These results establish the exotic properties of the chiral $d_1 + id_2$ superconducting state in doped graphene, which

if experimentally realized, will provide an exemplary playground for topological superconductivity. Furthermore, these results are also very important for any experimental scheme aimed at detecting the $d_1 + id_2$ state in graphene, as such scheme will likely be based on the distinctive properties of the edge.

We approximate the π -band structure of graphene as:

$$H_0 = -t \sum_{\langle i,j \rangle, \sigma} c_{i\sigma}^\dagger c_{j\sigma} + \mu \sum_i c_{i\sigma}^\dagger c_{i\sigma}, \quad (1)$$

where $t = 2.5$ eV is the nearest neighbor (NN) hopping amplitude and $c_{i\sigma}$ is the annihilation operator on site i with spin σ . The chemical potential is μ and the VHS appears at $\mu = \pm t$, where the Fermi surface transitions from being centered around K , K' to Γ . We study two different models for superconducting pairing from repulsive electron-electron interactions:

$$H_\Delta = \sum_{i,\alpha} \Delta_\alpha(i) (c_{i\uparrow}^\dagger c_{i+a_\alpha\downarrow}^\dagger - c_{i\downarrow}^\dagger c_{i+a_\alpha\uparrow}^\dagger) + \text{H.c.} \quad (2)$$

In the limit of very strong on-site Coulomb repulsion (mean-field) pairing appears on NN bonds such that $a_\alpha = \delta_\alpha$ ($\alpha = 1, 2, 3$) [1], whereas a moderate on-site repulsion gives rise to pairing on next-nearest-neighbor (NNN) bonds with $a_\alpha = \gamma_\alpha$ [2], see Fig. 1(a). The high electron density near the VHS efficiently screen long-range electron-electron interactions, and we also show that our results are largely independent on the choice of a . In mean-field theory the order parameter can be calculated from the condition $\Delta_\alpha(i) = -J \langle c_{i\downarrow} c_{i+a_\alpha\uparrow} - c_{i\uparrow} c_{i+a_\alpha\downarrow} \rangle$. Here J is the effective (constant) pairing potential arising from the electron-electron interactions and residing on NN bonds for $a = \delta$ and on NNN bonds for $a = \gamma$. Using this condition for Δ , the Hamiltonian $H = H_0 + H_\Delta$ can be solved self-consistently within the Bogoliubov-de Gennes formalism [4, 18]. The favored bulk solution of Δ_α belongs to the two-dimensional E_2 irreducible representation of the C_{6v} lattice point group. This representation can be expressed in the basis $\hat{a}_{d_1} = (1, -\frac{1}{2}, -\frac{1}{2})$, which has $d_1 = d_{x^2-y^2}$ symmetry when H_0 is diagonal, and

$\hat{a}_{d_2} = (0, \frac{\sqrt{3}}{2}, -\frac{\sqrt{3}}{2})$ which has $d_2 = d_{xy}$ symmetry, see Fig. 1(b). In the translational invariant bulk, these two solutions have the same T_c , but below T_c the complex combination $d_1 + id_2$ has the lowest free energy [1, 4]. There is also an s -wave solution, $\hat{a}_s = (1, 1, 1)$, but it only appears subdominantly and at very strong pairing.

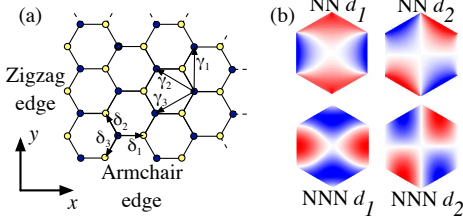


FIG. 1: (Color online) (a) Graphene with NN bonds δ_α , NNN bonds γ_α , zigzag and armchair edges indicated. (b) Different d -wave superconducting order parameters for NN and NNN pairing with negative (blue) and positive (red) sign.

In order to quantify the edge effects we study thick ribbons with both zigzag and armchair edges. We assume smooth edges and Fourier transform in the direction parallel to the edge. Due to computational limitations we need $J \gtrsim 0.5t$ in order to reach bulk conditions inside the slab. This gives rather large Δ_α , but by studying the J -dependence we can nonetheless draw conclusions for the experimentally relevant low- J regime.

Superconducting state at the edge.—In the bulk, the $d_1 + id_2$ state has a free energy ΔF lower than the $d_{1,2}$ states, which varies strongly with both doping and pairing potential, see inset in Fig. 2(c). However, sample edges break the translational invariance and a qualitatively different solution emerges. Figure 2(a) shows how the zigzag edge completely suppresses the imaginary part of Δ_α , while at the same time enhancing the magnitude. This suppression leads to a pure d_1 solution at the edge, an effect we quantify in Fig. 2(b) by plotting the d_1 -character $|\frac{\sqrt{2}}{\sqrt{3}}(\Delta_1 - \frac{1}{2}(\Delta_2 + \Delta_3))|^2$. The edge behavior can be understood by noting that bonds δ_2 and δ_3 (γ_2 and γ_3) are equivalent for both armchair and zigzag edges [19] and, therefore, the d_1 -wave state is heavily favored at both type of edges. Since the edge is of the zigzag type for edges with 30° and 90° angles off the x -axis and of the armchair type for 0° and 60° angles, we conclude that any edge should host d -wave order with nodes angled 45° from the edge direction. In order to quantify the spatial extent of this edge effect, we calculate a decay length ξ by fitting the d_1 -character profile to the functional form $(Ce^{-x/\xi} + 0.5)$ with $C \approx 0.5$. As seen in Fig. 2(c), ξ varies strongly with ΔF , but very little with edge type and doping level. Furthermore, the increase in ξ for NNN pairing compared to NN pairing suggests that the edge will be even more important in models with longer ranged Coulomb repulsion. The strongly increasing ξ with decreasing ΔF has far-reaching consequences for graphene. For example, $J = 0.5t$ and doping at the VHS gives $\xi \approx 25 \text{ \AA}$ for NN pairing. With an expected much weaker superconduct-

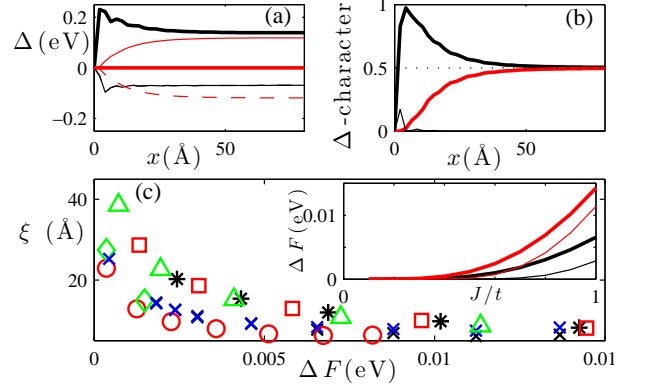


FIG. 2: (Color online) (a) Order parameter profile for the zigzag edge for NN $J = 0.75t$ at the VHS with real (black) and imaginary (red) part for Δ_1 (thick), Δ_2 (thin), and Δ_3 (dashed) [black dashed line is hidden behind black solid line since $\text{Re}(\Delta_2) \approx \text{Re}(\Delta_3)$]. (b) Character of the order parameter in (a): d_1 (thick black), d_2 (thick red), and s (thin black). Dotted line marks the bulk value. (c) Decay length ξ of the d_1 -character as function of ΔF for different doping levels, edges, and superconducting pairing: NN pairing, zigzag edge, and $\mu = t$ (black \times), $\mu = 0.8t$ (red \circ), $\mu = 1.2t$ (green \diamond) or armchair edge and $\mu = t$ (blue \times), NNN pairing, zigzag edge, and $\mu = t$ (black \star), $\mu = 0.8t$ (red \square), $\mu = 1.2t$ (green \triangle) [blue, \times symbols is often completely overlaying black, \times symbols since no notable difference is found between zigzag and armchair edges]. Inset shows ΔF as function of the pairing potential for NN pairing (black) and NNN pairing (red) for $\mu = t$ (thick) and $\mu = 1.2t$ (thin). $\mu < t$ has a ΔF curve similar to $\mu > t$.

ing pairing in real graphene, the edge will not only modify the properties of the superconducting state in graphene nanoribbons, but also in macroscopically sized graphene samples. We have verified that both the $d_1 + id_2$ state itself and edge effects described here are stable in the presence of random disorder [18].

Chiral edge states.—Any $d_1 + id_2$ state, even with one subdominant part, violates both time-reversal and parity symmetry and has been shown to host two chiral edge states [12, 14, 15]. The topological invariant guaranteeing the existence of these two chiral edge modes also causes quantized spin- and thermal-Hall responses [15, 16]. Figure 3(a) shows the band structure for a zigzag slab. The self-consistent solution (thick black) gives two Dirac cones located at $\pm k_0$, where bands with same velocities reside on the same surface, thus yielding two co-propagating chiral surface states per edge. The band structure for the constant (non-self-consistent) bulk $d_1 + id_2$ state also has two Dirac cones (thin black), but shifted away from k_0 . The shift is directly related to the d_1 state at the edge. The d_1 state has no surface states on the zigzag edge, only bulk nodal quasiparticles, where the nodes for a d_1 order parameter with amplitude equal to that on the edge are located at $\pm k_0$ (thin red). The similarity between the $d_1 + id_2$ and d_1 edge band structures thus makes for only modest effects of the edge on the self-consistent band structure. It also results in the chiral edge modes being well localized to the edge, as seen in the local density of states (LDOS) plot in

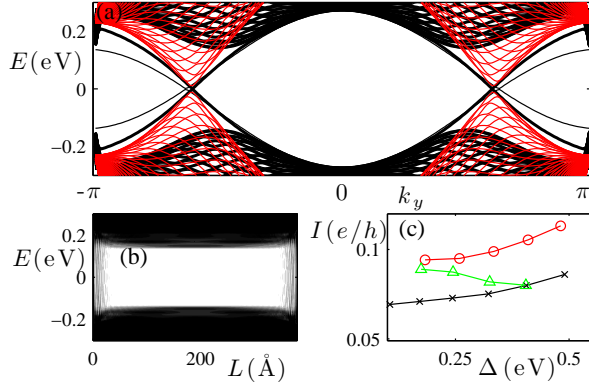


FIG. 3: (Color online) (a) Band structure for a zigzag edge slab with NN $J = 0.75t$, $\mu = t$, and self-consistent Δ (thick black), constant $d_1 + id_2$ state corresponding to the bulk state (thin black), and constant d_1 state corresponding in amplitude to the d_1 state at the surface. (b) LDOS across the ribbon for the self-consistent solution in (a) interpolating between 0.2 (black) to 0 (white) states/eV/unit cell, showing a bulk gap of 0.18 eV and gapless edge states. (c) Quasiparticle edge current in units of e/h as function of superconducting bulk order parameter $\Delta(1, e^{2\pi i/3}, e^{4\pi i/3})$ for zigzag edge with $\mu = t$ (black \times), $\mu = 0.8t$ (red \circ), and armchair edge with $\mu = t$ (green \triangle).

Fig. 3(b). The constant edge LDOS is a consequence of the one-dimensional Dirac spectrum. We note especially that no d -wave superconducting graphene edge will display a zero-bias conductance peak due to zero-energy surface states, in contrast to the cuprate superconductors [13]. Such a peak is only present when the order parameter for incidence angle θ on the edge has a different sign from when the angle is $\pi - \theta$. This only happens for the d_2 -solution on both the zigzag and armchair edge.

The breaking of time-reversal symmetry gives rise to spontaneous edge currents carried by the chiral edge modes [12–14, 16]. By combining the charge continuity equation with the Heisenberg equation for the particle density [4], we calculate in Fig. 3(c) the quasiparticle edge current as function of of the bulk order parameter $\Delta(1, e^{2\pi i/3}, e^{4\pi i/3})$. We find no evidence for a quantized boundary current equal to $2e\Delta/h$, as previously suggested [14]. In fact, we find a non-linear relationship between current and Δ , a strong variation with doping level, and, most importantly, the armchair current even *decreases* when Δ increases. The last result can be understood by studying the zero-energy crossing $\pm k_0$ of the chiral edge modes. For the zigzag edge k_0 increases with increasing Δ , whereas for the armchair edge k_0 decreases. In general, we find that changes in current are proportional to δk_0^β with $\beta \approx 1 - 2$. This, at least, partially agree with earlier results reporting a $\beta = 2$ dependence [12]. Finite k -point sampling and neglecting the screening supercurrents could potentially explain the discrepancy.

Majorana mode.—Heavy doping of graphene, by either adatom deposition [2] or gating [3], breaks the $z \rightarrow -z$ mirror

symmetry and introduces a Rashba spin-orbit coupling [20]

$$H_\lambda = i\lambda_R \sum_{\langle i,j \rangle, \sigma, \sigma'} \hat{z} \cdot (\mathbf{s}_{\sigma, \sigma'} \times \hat{\mathbf{d}}_{ij}) c_{i\sigma}^\dagger c_{j\sigma'}, \quad (3)$$

where $\hat{\mathbf{d}}_{ij}$ is the unit vector from site j to i . Superconducting two-dimensional systems with Rashba spin-orbit coupling and magnetic field have recently attracted much attention due to the possibility of creating Majorana fermions at vortex cores or edges [5, 21, 22]. At edges the Majorana fermion appears as a single mode crossing the bulk gap. This should be contrasted with the behavior found above, where the edge instead hosts two modes. We will here show that a Majorana mode is created in d -wave superconducting doped graphene in the presence a moderate Zeeman field: $H_h = -h_z \sum_i (c_{i\uparrow}^\dagger c_{i\uparrow} - c_{i\downarrow}^\dagger c_{i\downarrow})$. Due to spin-mixing in H_λ , the basis vector $X^\dagger = (c_{i\uparrow}^\dagger c_{i\downarrow}^\dagger c_{i\uparrow} c_{i\downarrow})$ has to be used when expressing the Hamiltonian $H_{\text{ext}} = H_0 + H_\Delta + H_\lambda + H_h$ in matrix form: $H_{\text{ext}} = \frac{1}{2} X^\dagger \mathcal{H}_{\text{ext}} X$. This results in a doubling of the number of eigenstates compared to the physical band structure. This doubling is necessary for the appearance of the Majorana fermion, since a regular fermion consists of two Majorana fermions.

A change in the number of edge modes marks a topological phase transition which, in general, can only occur when the bulk energy gap closes. We therefore start by identify the conditions for bulk zero energy solutions of H_{ext} . Close to the VHS we can, to a first approximation, use only the partially occupied π -band for small Δ , λ_R , and h_z . A straightforward calculation [5] for this one-band Hamiltonian gives the following bulk-gap closing conditions at $\mu \sim t$:

$$(\mu - t|\epsilon_k|)^2 + \Delta_k^2 = h_z^2 + \lambda_R^2 |\mathcal{L}_k|^2, \quad |\Delta_k| |\lambda_R \mathcal{L}_k| = 0, \quad (4)$$

where $\epsilon_k = \sum_\alpha e^{ik\delta_\alpha}$ is the band structure, $\varphi_k = \arg(\epsilon_k)$, $\Delta_k = -\sum_\alpha \Delta_\alpha \cos(k\delta_\alpha - \varphi_k)$ is the k -dependent intra-band superconducting order for NN pairing [1], and $\mathcal{L}_k = \text{Im}[e^{-i\varphi_k} (-\frac{\sqrt{3}}{2} e^{ik\delta_2} + \frac{\sqrt{3}}{2} e^{ik\delta_3}, e^{ik\delta_1} - \frac{1}{2} e^{ik\delta_2} - \frac{1}{2} e^{ik\delta_3}, 0)]$ is the spin-orbit interaction when expressed in the form $H_\lambda = \sum_{k\sigma\sigma'} \lambda_R \mathcal{L}_k \cdot \mathbf{s}_{\sigma\sigma'} c_{k\sigma}^\dagger c_{k\sigma'}$ for the one-band model. Equations (4) are met at Γ , K , and M in the Brillouin zone, where they produce the conditions $(\mu - 3t)^2 = h_z^2$, $\mu^2 = h_z^2$, and $(\mu - t)^2 + \Delta_k^2(M) = h_z^2$, respectively. At $\mu \sim t$ only the last condition is satisfied for small h_z , which is necessary for superconductivity to survive. We find $\Delta_k(M) = 2\Delta$ for the $\Delta(1, e^{2\pi i/3}, e^{4\pi i/3})$ order parameter and, thus, at the VHS there is a topological phase transition at $h_c = 2\Delta$. Figure 4(a) shows how the eigenvalue spectrum of a superconducting zigzag slab at the VHS develops when h_z is swept past h_c . At finite λ_R and/or h_z the chiral modes in Fig. 3(a) split with one mode moving towards $k_y = 0$ and the other one towards the zone boundary at $k_y = \pi$, see left-most figure in Fig. 4(a). At h_c (center figure) the bulk gap closes at both $k_y = 0, \pi$. The closure at $k_y = \pi$ annihilates the outer chiral modes whereas the closure at $k_y = 0$ leaves a new Dirac cone

crossing the bulk band gap with the two modes belonging to different edges. Thus, at $h_z > h_c$ we are left with three modes per edge crossing the bulk gap. The odd number establishes the existence of a Majorana mode alongside the two remnant chiral modes. Figure 4(b) shows how Δ develops in the pres-

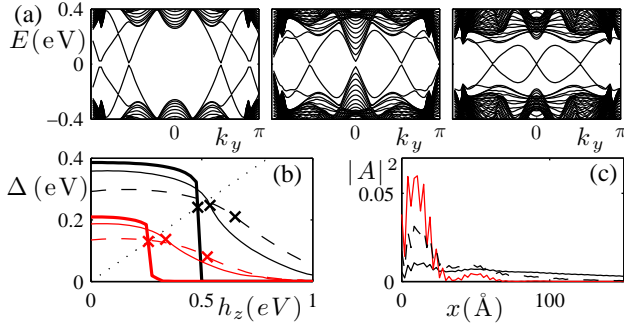


FIG. 4: (Color online) (a) Eigenvalue spectrum for a zigzag slab with $NN J = 1.2t$, $\mu = t$, $\lambda_R = 0.2t$, and $h_z = 0.4, 0.535$ and 0.6 eV (left to right), with $h_c = 0.535$ eV. Small gaps in the surface states are due to limited k -point sampling. (b) Self-consistent Δ as function of h_z for $J = 1.2t$ (black), $0.9t$ (red) for $\lambda_R = 0.05t$ (thick), $0.2t$ (thin), and $0.3t$ (dashed). Dotted line mark the $h_c = 2\Delta$ one-band model phase transition. Crosses mark the numerical phase transition. (c) Eigenvalue amplitude squared for the Majorana mode in (a) for $h_z = 0.54$ eV (black), 0.56 (dashed), and 0.6 (red).

ence of an applied Zeeman field h_z , with \times -symbols marking the phase transition into the phase with a Majorana fermion. The dotted line marks the one-band result $h_c = 2\Delta$, which is a good approximation for small λ_R . In this small λ_R -regime there is a very pronounced drop in Δ at the phase transition with only a small remnant superconducting state in the Majorana phase at $h_z > h_c$, which results in a poorly resolved Majorana mode. Larger λ_R gives a stronger superconducting state in the Majorana phase. However, for $\lambda_R > 0.2t$ we find $h_c > 2\Delta$, and the superconducting state is again very weak beyond the phase transition. We thus conclude that, in order to create a Majorana fermion at the edge of d -wave superconducting graphene doped very close to the VHS, a small to moderate Rashba spin-orbit coupling, $\lambda_R \sim 0.2t$, and a Zeeman field of the order of 2Δ is needed. With reported tunability with electric field [24], as well as impurity-induced Rashba spin-orbit coupling [25], $\lambda_R \sim 0.2t$ is likely within experimental reach in heavily doped graphene. The Zeeman field can be generated by proximity to a ferromagnetic insulator, whereas if applying an external magnetic field, orbital effects also needs to be taken into account. Finally, in Fig. 4(c) we plot the spatial profile of the Majorana mode amplitude just beyond h_c . Due to the larger Δ at the edge, the bulk enters the Majorana-supporting topological phase before the edge. Therefore, the Majorana mode does not appear at the edge but is spread throughout the sample for $h_z \gtrsim h_c$. Not until $h_z > 2\Delta(\text{edge})$ does the Majorana mode appear as a pure edge excitation.

In summary, we have shown that the $d_1 + id_2$ superconduct-

ing state in heavily doped graphene is in a pure d_1 state on any edge. The d_1 edge state significantly modifies the superconducting state even in macroscopic graphene samples due to a long decay length. Moreover, $d_1 + id_2$ superconducting graphene hosts two well-localized chiral edge modes, which carry a non-quantized spontaneous quasiparticle current. A Majorana mode can also be created at the edge by tuning a moderate Zeeman field. These results establish the properties of the $d_1 + id_2$ state in graphene, and will be important for any experimental detection of this state.

The author thanks A. V. Balatsky, M. Fogelström, and T. H. Hansson for discussions and the Swedish research council (VR) for support.

-
- [1] K. S. Novoselov, A. K. Geim, S. V. Morozov, D. Jiang, Y. Zhang, S. V. Dubonos, I. V. Grigorieva, and A. A. Firsov, *Science* **306**, 666 (2004).
 - [2] J. L. McChesney, A. Bostwick, T. Ohta, T. Seyller, K. Horn, J. González, and E. Rotenberg, *Phys. Rev. Lett.* **104**, 136803 (2010).
 - [3] D. K. Efetov and P. Kim, *Phys. Rev. Lett.* **105**, 256805 (2010).
 - [4] R. Nandkishore, L. S. Levitov, and A. V. Chubukov, *Nat. Phys.* **8**, 158 (2011).
 - [5] M. Kiesel, C. Platt, W. Hanke, D. A. Abanin, and R. Thomale, *Phys. Rev. B* **86**, 020507(R) (2012).
 - [6] W.-S. Wang, Y.-Y. Xiang, Q.-H. Wang, F. Wang, F. Yang, and D.-H. Lee, *Phys. Rev. B* **85**, 035414 (2012).
 - [7] A. M. Black-Schaffer and S. Doniach, *Phys. Rev. B* **75**, 134512 (2007).
 - [8] C. Honerkamp, *Phys. Rev. Lett.* **100**, 146404 (2008).
 - [9] S. Pathak, and V. B. Shenoy, and G. Baskaran, *Phys. Rev. B* **81**, 085431 (2010).
 - [10] T. Ma, and Z. Huang, and F. Hu, and H.-Q. Lin, *Phys. Rev. B* **84**, 121410(R) (2011).
 - [11] J. González, *Phys. Rev. B* **78**, 205431 (2008).
 - [12] G. E. Volovik, *JETP Lett.* **66**, 522 (1997).
 - [13] M. Fogelström, D. Rainer, and J. A. Sauls, *Phys. Rev. Lett.* **79**, 281 (1997).
 - [14] R. B. Laughlin, *Phys. Rev. Lett.* **80**, 5188 (1998).
 - [15] T. Senthil, J. B. Marston, and M. P. A. Fisher, *Phys. Rev. B* **60**, 4245 (1999).
 - [16] B. Horovitz and A. Golub, *Phys. Rev. B* **68**, 214503 (2003).
 - [17] A. M. Black-Schaffer and S. Doniach, *Phys. Rev. B* **78**, 024504 (2008).
 - [18] See supplementary material for additional information.
 - [19] A. M. Black-Schaffer and S. Doniach, *Phys. Rev. B* **79**, 064502 (2009).
 - [20] C. L. Kane and E. J. Mele, *Phys. Rev. Lett.* **95**, 146802 (2005).
 - [21] J. D. Sau, R. M. Lutchyn, S. Tewari, and S. Das Sarma, *Phys. Rev. Lett.* **104**, 040502 (2010).
 - [22] J. Alicea, *Phys. Rev. B* **81**, 125318 (2010).
 - [23] M. Sato, Y. Takahashi, and S. Fujimoto, *Phys. Rev. B* **82**, 134521 (2010).
 - [24] H. Min, J. E. Hill, N. A. Sinitsyn, B. R. Sahu, L. Kleinman, and A. H. MacDonald, *Phys. Rev. B* **74**, 165310 (2006).
 - [25] A. H. Castro Neto and F. Guinea, *Phys. Rev. Lett.* **103**, 026804 (2009).

Supplementary material

In this supplementary material we provide: (1) a detailed, largely self-contained, description of the method underlying our results, and (2) numerical data showing the relative robustness of the bulk $d_1 + id_2$ superconducting state and its edge properties in the presence of disorder.

Method.— As described in the main text, we use the Hamiltonian $H = H_0 + H_\Delta$, where

$$H_0 = -t \sum_{\langle i,j \rangle, \sigma} c_{i\sigma}^\dagger c_{j\sigma} + \mu \sum_i c_{i\sigma}^\dagger c_{i\sigma}, \quad (5)$$

$$H_\Delta = \sum_{i,\alpha} \Delta_\alpha(i) (c_{i\uparrow}^\dagger c_{i+a_\alpha\downarrow}^\dagger - c_{i\downarrow}^\dagger c_{i+a_\alpha\uparrow}^\dagger) + \text{H.c.} \quad (6)$$

Here $c_{i\sigma}$ is the annihilation operator on site i of the honeycomb lattice with spin σ , $t = 2.5$ eV is the nearest-neighbor (NN) hopping amplitude, and μ is the chemical potential, where $\mu = \pm t$ corresponds to the van Hove singularities (VHSs) (H is particle-hole symmetric so hole and electron doping give the same result). Furthermore, the superconducting order parameter Δ_α resides on NN bonds when $a_\alpha = \delta_\alpha$ and on next-nearest neighbor (NNN) bonds when $a_\alpha = \gamma_\alpha$, where $\alpha = 1, 2, 3$ labels the three inequivalent bond directions, see Fig. 1(a) in the main text. Within mean-field theory, Δ_α is defined by the self-consistent condition:

$$\Delta_\alpha(i) = -J \langle c_{i\downarrow} c_{i+a_\alpha\uparrow} - c_{i\uparrow} c_{i+a_\alpha\downarrow} \rangle, \quad (7)$$

where J is the effective pairing potential on NN bonds for $a = \delta$ and on NNN bonds for $a = \gamma$. J is a consequence of the local repulsive Coulomb interaction, which in the limit of very strong on-site repulsion results in pairing on NN bonds [1] whereas a moderate on-site repulsion results in NNN bond pairing [2].

We can solve H within the Bogoliubov-de Gennes formalism by writing

$$H = X^\dagger \mathcal{H} X \quad \text{with} \quad X^\dagger = (c_{i,\uparrow}^\dagger, c_{i,\downarrow}), \quad (8)$$

and diagonalizing the matrix \mathcal{H} to find all eigenvalues E^ν and eigenvectors V^ν , where $\nu = 1, \dots, 2N$ for N sites. We can then define new operators $Y^\dagger = (\gamma_\nu^\dagger)$ using $X = \mathcal{V}Y$ with the columns of \mathcal{V} given by the eigenvectors V^ν , such that the Hamiltonian H is diagonal in these new operators: $H = \sum_\nu E^\nu \gamma_\nu^\dagger \gamma_\nu$. A self-consistent solution scheme start with first guessing the value of Δ_α , diagonalizing \mathcal{H} for this value, using the self-consistent condition Eq. (7) to recalculate Δ_α from the eigenvalues and eigenvectors, and then reiterate these steps until the order parameter Δ_α within two subsequent steps changes less than a small predetermined convergence limit. Using the self-consistent value for Δ_α any electronic property of the system can be calculated in using the eigenbasis. For example, the local density of states (LDOS) can be calculated as

$$D_i(E) = \sum_\nu |V_i^\nu|^2 \delta(E - E^\nu) + |V_{N+i}^\nu|^2 \delta(E + E^\nu), \quad (9)$$

where the first part is the spin-up contribution and the second part the spin-down contribution. Numerically, we use a small Gaussian broadening for the δ -functions. We are also interested in the quasiparticle current, which can be calculated using the continuity equation for the charge current density \mathbf{J} :

$$\nabla \cdot \mathbf{J} + \frac{\partial \rho}{\partial t} = 0 \quad (10)$$

together with the Heisenberg equation for the particle density per unit cell n_i :

$$\frac{dn_i}{dt} = \frac{i}{\hbar} [H, n_i], \quad (11)$$

where $\rho = e\langle n \rangle$ [3, 4]. The quantum average of the commutator in Eq. (11) can easily be shown to only contain H_0 for a self-consistent solution of Δ_α . The total quasiparticle edge current is then simply $I = \sum \mathbf{J}_{||}$, where the summation is over all unit cells at the edge with a finite \mathbf{J} parallel to the edge.

The above formalism can be applied to any structure on the honeycomb lattice. In order to investigate edge properties, we study H on thick graphene ribbons having either zigzag or armchair edges. We make sure that the ribbons are always thick enough to guarantee bulk conditions in the interior. For simplicity, we assume smooth edges so we can Fourier transform in the direction along the edge, which introduces a k -point index, while reducing the site index i to only enumerate sites perpendicular to the edge, i.e. i now only measures the distance to the edge.

We also study the influence of a finite Rashba spin-orbit coupling:

$$H_\lambda = i\lambda_R \sum_{\langle i,j \rangle, \sigma, \sigma'} \hat{z} \cdot (\mathbf{s}_{\sigma, \sigma'} \times \hat{\mathbf{d}}_{ij}) c_{i\sigma}^\dagger c_{j\sigma'}, \quad (12)$$

where $\hat{\mathbf{d}}_{ij}$ is the unit vector from site j to i , in combination with a Zeeman field:

$$H_h = -h_z \sum_i (c_{i\uparrow}^\dagger c_{i\uparrow} - c_{i\downarrow}^\dagger c_{i\downarrow}). \quad (13)$$

The spin-mixing in the Rashba term now requires us to write $H_{\text{ext}} = H_0 + H_\Delta + H_\lambda + H_h$ as

$$H_{\text{ext}} = \frac{1}{2} X^\dagger \mathcal{H}_{\text{ext}} X \quad \text{with} \quad X^\dagger = (c_{i\uparrow}^\dagger c_{i\downarrow}^\dagger c_{i\uparrow} c_{i\downarrow}), \quad (14)$$

i.e. we need to double the number of eigenstates compared to the physical band structure. This is expected since a Majorana fermion is essentially half a fermion. By applying the same self-consistent procedure described above to H_{ext} , we can solve for the superconducting order parameter Δ , calculate all physical observables such as the LDOS, and also calculate the eigenvalue spectrum, which contains the Majorana mode for a large enough field h_z . The Majorana mode appears when the eigenvalue spectrum develops from having an even number of edge modes to an odd number. Such a change in the number of edge modes is in general always associated with the closing of the bulk gap. We can analytically extract the approximate bulk gap closing condition from an effective one-band model. The kinetic Hamiltonian H_0 is diagonalized in the bulk by changing the basis from the site-operators $\{c_A, c_B\}$ on the two inequivalent sites A and B , to the band operators $\{a, b\}$ through:

$$\begin{pmatrix} c_{Ak\sigma} \\ c_{Bk\sigma} \end{pmatrix} = \frac{1}{\sqrt{2}} \begin{pmatrix} a_{k\sigma} + b_{k\sigma} \\ e^{-i\varphi_k} (a_{k\sigma} - b_{k\sigma}) \end{pmatrix}. \quad (15)$$

Here $a_{k\sigma}^\dagger$ creates an electron in the lower π -band and $b_{k\sigma}^\dagger$ creates an electron in the upper π -band, such that

$$H_0 = \sum_{k\sigma} \left[(\mu - t\epsilon_k) a_{k\sigma}^\dagger a_{k\sigma} + (\mu + t\epsilon_k) b_{k\sigma}^\dagger b_{k\sigma} \right], \quad (16)$$

where the k -dependence of the π -bands is given by $\epsilon_k = |\sum_\alpha e^{ik \cdot \delta_\alpha}|$ and $\varphi_k = \arg(\sum_\alpha e^{ik \cdot \delta_\alpha})$. We will for simplicity now assume $\mu \sim t$ and focus on the lower π -band, but the same calculation is also valid for doping levels around the VHS at $\mu = -t$. By only keeping terms within the lower band, ignoring effects in the upper band along with any cross-terms, we arrive at:

$$\begin{aligned} H'_z &= -h_z \sigma \sum_k a_{k\sigma}^\dagger a_{k\sigma} \\ H'_\Delta &= - \sum_{k, \alpha} \Delta_\alpha \cos(k \cdot \delta_\alpha - \varphi_k) (a_{k\uparrow}^\dagger a_{-k\downarrow}^\dagger) + \text{H.c.} \\ H'_\lambda &= \sum_{k\sigma\sigma'} \mathcal{L}_k \cdot \mathbf{s}_{\sigma\sigma'} a_{k\sigma}^\dagger a_{k\sigma'}, \end{aligned} \quad (17)$$

where $\mathcal{L}_k = \lambda_R \text{Im}[e^{-i\varphi_k} (-\frac{\sqrt{3}}{2} e^{ik\delta_2} + \frac{\sqrt{3}}{2} e^{ik\delta_3}, e^{ik\delta_1} - \frac{1}{2} e^{ik\delta_2} - \frac{1}{2} e^{ik\delta_3}, 0)]$. The one-band Bogoliubov-de Gennes Hamiltonian $H'_{\text{ext}} = H'_0 + H'_\Delta + H'_z + H'_\lambda$ can now be diagonalized and we find the eigenvalues

$$E(k) = \sqrt{(\mu - t\epsilon_k)^2 + \lambda_R^2 \mathcal{L}_k^2 + h_z^2 + |\Delta_k|^2 \pm 2\sqrt{(\mu - t\epsilon_k)^2 \lambda_R^2 \mathcal{L}_k^2 + [(\mu - t\epsilon_k)^2 + |\Delta_k|^2] h_z^2}}, \quad (18)$$

where $\Delta_k = \sum_\alpha \Delta_\alpha \cos(k \cdot \delta_\alpha - \varphi_k)$. Following the procedure in Ref. 5, the zero energy values of Eq. (18), or equivalently the bulk-gap closing condition, satisfy

$$(\mu - t|\epsilon_k|)^2 + \Delta_k^2 = h_z^2 + \lambda_R^2 |\mathcal{L}_k|^2, \quad |\Delta_k| |\lambda_R \mathcal{L}_k| = 0, \quad (19)$$

which is the same as Eq. (4) in the main text. From this equation we locate the only low-field bulk closing point to be at $(\mu - t)^2 + \Delta_k^2(M) = h_z^2$, where $\Delta_k(M) = 2\Delta$ for the $\Delta(1, e^{2\pi i/3}, e^{4\pi i/3})$ order parameter. As seen in Fig. 4(b) in the main text this approximative bulk closing condition is accurate for small to moderately large λ_R .

Disorder effects.— Heavy doping of graphene will undoubtedly introduce some amount of disorder into the system. Disorder can affect the results derived in this Letter in several ways. First of all, sufficiently strong disorder will suppress the superconducting order parameter, this is especially true in non- s -wave superconductors. Secondly, disorder breaks the translational invariance and, thus, the two d -wave channels in graphene are no longer guaranteed to be degenerate. Related to this is the fact that there exists also an extended s -wave solution, which, in general, is heavily disfavored but in the presence of disorder might become more important. In addition to these bulk effects, disorder might also influence the edge properties of the $d_1 + id_2$ state.

In order to study the effect of disorder we model both the bulk and zigzag edges in the presence of Anderson disorder, i.e. a locally fluctuating chemical potential:

$$H_{0,\text{dis}} = -t \sum_{\langle i,j \rangle, \sigma} c_{i\sigma}^\dagger c_{j\sigma} + \sum_i (\mu + \delta\mu_i) c_{i\sigma}^\dagger c_{i\sigma}, \quad (20)$$

where the local chemical potential variations $\delta\mu_i$ are distributed randomly within the interval $[-W, W]$, with W being the disorder strength. This type of disorder model captures the effect of local charge inhomogeneities introduced by the doping. It is also reasonable to assume, as is done here, that the disorder will in general be directionally independent, such that it does not single out one bond direction over the other. We solve $H_{0,\text{dis}} + H_\Delta$ for multiple disorder configurations in large bulk and edge samples and study how the superconducting order evolves with the disorder strength W . We fix $\mu = 1$ which maximizes the effect of the disorder, since both negative and positive deviations from the VHS causes the superconducting order parameter to decrease. In Fig. 5(c) we plot on the right axis the superconducting order parameter Δ_1 as function of the NN pairing

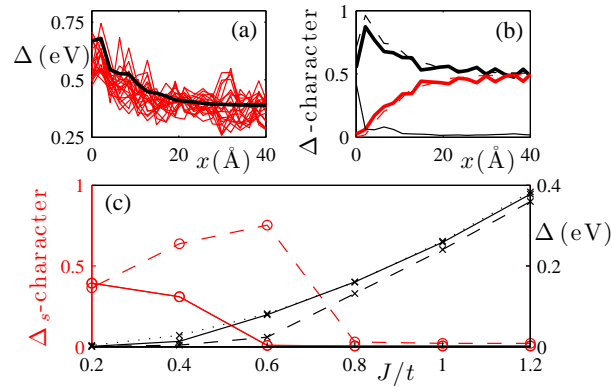


FIG. 5: (Color online) (a) Order parameter Δ_1 profiles at the zigzag edge for NN $J = 1.2t$ at the VHS for a 20 unit cell wide sample with $W = 0.5t = 1$ eV disorder (red). Clean sample (thick black). (b) Average character of the order parameter in (a): d_1 (thick black), d_2 (thick red), and s (thin black). Dashed lines display the clean d_1 and d_2 results, respectively. (c) Bulk Δ_1 order parameter (right, black axis) as function of NN J for clean (black dotted), $W = 0.2t = 0.5$ eV (black solid), and $W = 0.5t = 1$ eV (black dashed) and the corresponding s -wave character (left, red axis).

potential J for a 40×40 Å bulk sample. The results are averaged over as many as 20 different disorder configurations. For $W = 0.2t = 0.5$ eV there is a suppression of the superconducting state for $J \leq 0.4t$, at which point the character of the superconducting state also changes from perfect $d_1 + id_2$ to contain a significant amount of s -wave character (right axis). At $J = 0.4t$, W is 18 times larger than Δ_1 and thus the $d_1 + id_2$ state survives disorder at least an order of a magnitude stronger than the superconducting gap. The appearance of a sizable s -wave component at very strong disorder is expected since isotropic states are more robust against disorder, but this also suppresses the overall superconducting order parameter. For $W = 0.4t = 1$ eV we find the same scenario, with the $d_1 + id_2$ state being suppressed into a weaker partial s -wave state at $J \leq 0.6t$, where W is 12 times larger than Δ_1 . Based on these results, we expect the $d_1 + id_2$ state to survive essentially unchanged in the bulk in the presence of even moderately strong disorder. In Figs. 5(a,b) we plot the behavior at the edge for a representative $W = 1$ eV disorder configuration. Computational demands limit the size of the sample and we are forced to use a rather large $J = 1.2t$. Nonetheless, the disorder strength is still in this case almost 3 times larger than the bulk Δ_1 value. The Δ_1 profile into the sample in Fig. 5(a) shows a noticeable spatial variation, but still, the average is not suppressed much from the clean limit. As seen in Fig. 5(b), the average character of the superconducting state is also essentially left unchanged by this relatively strong disorder. We thus conclude that even moderately strong disorder does not influence the edge properties of the $d_1 + id_2$ superconducting state in heavily doped graphene.

-
- [1] A. M. Black-Schaffer and S. Doniach, Phys. Rev. B **75**, 134512 (2007).
 - [2] M. Kiesel, C. Platt, W. Hanke, D. A. Abanin, and R. Thomale, arXiv:1109.2953 (unpublished).
 - [3] L. Covaci and F. Marsiglio, Phys. Rev. B **73**, 014503 (2006).
 - [4] A. M. Black-Schaffer and S. Doniach, Phys. Rev. B **78**, 024504 (2008).
 - [5] M. Sato, Y. Takahashi, and S. Fujimoto, Phys. Rev. B **82**, 134521 (2010).